Disruption of CXCR4 signaling in pharyngeal neural crest cells causes DiGeorge syndrome-like malformations

S. Escot, C. Blavet, Emmanuel Faure, S. Zaffran, Jean-Loup Duband, Claire Fournier-Thibault

© 2016. Published by The Company of Biologists Ltd | Development (2016) 143, 582-588 doi:10.1242/dev.126573

RESEARCH REPORT

Disruption of CXCR4 signaling in pharyngeal neural crest cells causes DiGeorge syndrome-like malformations

Sophie Escot[1,2,*], Cédrine Blavet[1,2,§], Emilie Faure[3,4,§], Stéphane Zaffran[3,4], Jean-Loup Duband[1,2,‡,¶] and Claire Fournier-Thibault[1,2,¶]

ABSTRACT

DiGeorge syndrome (DGS) is a congenital disease causing cardiac outflow tract anomalies, craniofacial dysmorphogenesis, thymus hypoplasia, and mental disorders. It results from defective development of neural crest cells (NCs) that colonize the pharyngeal arches and contribute to lower jaw, neck and heart tissues. Although *TBX1* has been identified as the main gene accounting for the defects observed in human patients and mouse models, the molecular mechanisms underlying DGS etiology are poorly identified. The recent demonstrations that the SDF1/CXCR4 axis is implicated in NC chemotactic guidance and impaired in cortical interneurons of mouse DGS models prompted us to search for genetic interactions between *Tbx1*, *Sdf1* (*Cxcl12*) and *Cxcr4* in pharyngeal NCs and to investigate the effect of altering CXCR4 signaling on the ontogeny of their derivatives, which are affected in DGS. Here, we provide evidence that *Cxcr4* and *Sdf1* are genetically downstream of *Tbx1* during pharyngeal NC development and that reduction of CXCR4 signaling causes misrouting of pharyngeal NCs in chick and dramatic morphological alterations in the mandibular skeleton, thymus and cranial sensory ganglia. Our results therefore support the possibility of a pivotal role for the SDF1/CXCR4 axis in DGS etiology.

KEY WORDS: Neural crest, CXCR4, SDF1, TBX1, DiGeorge syndrome, Chick, Mouse

INTRODUCTION

DiGeorge or velocardiofacial syndrome (DGS) is a congenital disease characterized by cardiovascular defects, craniofacial anomalies, thymus hypoplasia, mental disorders and dysphagia (Shprintzen, 2008). It results primarily from defective development of cranial and cardiac neural crest cells (NCs) that invade the first four pharyngeal arches (PA1-4) and contribute to the formation of the lower jaw, the neck and the heart (Le Douarin and Kalcheim, 1999). In chick, ablation of this pharyngeal NC population phenocopies the cardiocraniofacial anomalies found in DGS patients (Kirby et al., 1983). DGS is caused by hemizygous deletions within chromosome 22q11.2, which have been reproduced on chromosome 16 in the *Df1/+* and *LgDel/+* mouse models (Puech et al., 1997). The Df1 and LgDel regions carry *Tbx1*, for which deletion and complementation studies in mouse indicate that it is responsible for many of the abnormalities observed (Lindsay et al., 2001). In human, *TBX1* maps to the 22q11 region and its haploinsufficiency or sequence mutations have been found in DGS patients (Scambler, 2010). During mouse development, *Tbx1* is first expressed in pharyngeal endoderm and ectoderm and then in the PA mesoderm (Garg et al., 2001; Zhang et al., 2005; Mesbah et al., 2012). However, though not expressed by pharyngeal NCs, loss of *Tbx1* impairs their migration and differentiation (Kochilas et al., 2002; Vitelli et al., 2002; Calmont et al., 2009).

Malformations in DGS patients are highly variable, suggesting that complex genetic interactions are involved (Shprintzen, 2008; Scambler, 2010). Despite progress in the identification of *Tbx1* targets, the molecular mechanisms involved in pharyngeal NC development that could account for DGS etiology have not been completely elucidated. Interestingly, signaling by CXCR4, a receptor for the chemokine stromal derived factor 1 (SDF1, also named CXCL12), is deficient in brain cortical interneurons of mouse DGS models, resulting in their abnormal migration, probably accounting for the mental disorders observed in DGS patients (Meechan et al., 2012; Toritsuka et al., 2013). Loss of *Cxcr4* or *Sdf1* in mouse causes cardiac anomalies similar to those observed in DGS (Ma et al., 1998) and disruption of SDF1/CXCR4 signaling in chick demonstrated that these cardiac defects result from abnormal migration of cardiac NCs (Escot et al., 2013). In addition, the *Cxcr4* promoter harbors putative TBX1 binding sites (Castellanos et al., 2014). Together, these observations raise the possibility that, in addition to cortical interneurons in the brain, CXCR4 signaling could regulate pharyngeal NC migration and that its misregulation could ultimately cause many of the cardiocraniofacial defects associated with DGS.

RESULTS AND DISCUSSION

Sdf1 and *Cxcr4* expression levels are diminished in *Tbx1* mutant mice

To investigate whether *Sdf1* and *Cxcr4* might be *Tbx1* targets, we analyzed their expression profiles in mouse embryos at the time of pharyngeal NC migration, by *in situ* hybridization and using a transgenic *Cxcr4*-EGFP mouse line (Tran et al., 2007). Analysis of whole embryos (Fig. 1Aa-Ad) and cross-sections through PA2 (Fig. 1Ae-Ah) at embryonic day (E) 9.5 showed *Cxcr4* expression in streams of cells along the ectoderm identified as migrating NCs by the marker *Sox10*. *Sdf1* was conspicuous in the ectoderm and pharyngeal endoderm in proximity to the migrating NCs. Interestingly, *Tbx1* was expressed in the same regions of pharyngeal endoderm and lateral ectoderm as *Sdf1* (Fig. 1Ad,

[1]Université Pierre et Marie Curie, Laboratoire de Biologie du Développement, Paris 75252 Cedex 5, France. [2]CNRS, Laboratoire de Biologie du Développement, Paris 75252 Cedex 5, France. [3]Aix Marseille Université, GMGF UMRS910, Faculté de Médecine, 27 Bd Jean Moulin, Marseille 13385, France. [4]Inserm U910, Faculté de Médecine, 27 Bd Jean Moulin, Marseille 13005, France.
*Present address: Max-Delbrück-Centrum für Molekulare Medizin, Berlin, Germany. ‡Present address: Institut Mondor de Recherche Biomédicale, Créteil, France.
§These authors contributed equally to this work

¶Authors for correspondence (claire.thibault@upmc.fr; jean-loup.duband@inserm.fr)

Received 18 May 2015; Accepted 4 January 2016

Development (2016) 143, 582-588 doi:10.1242/dev.126573

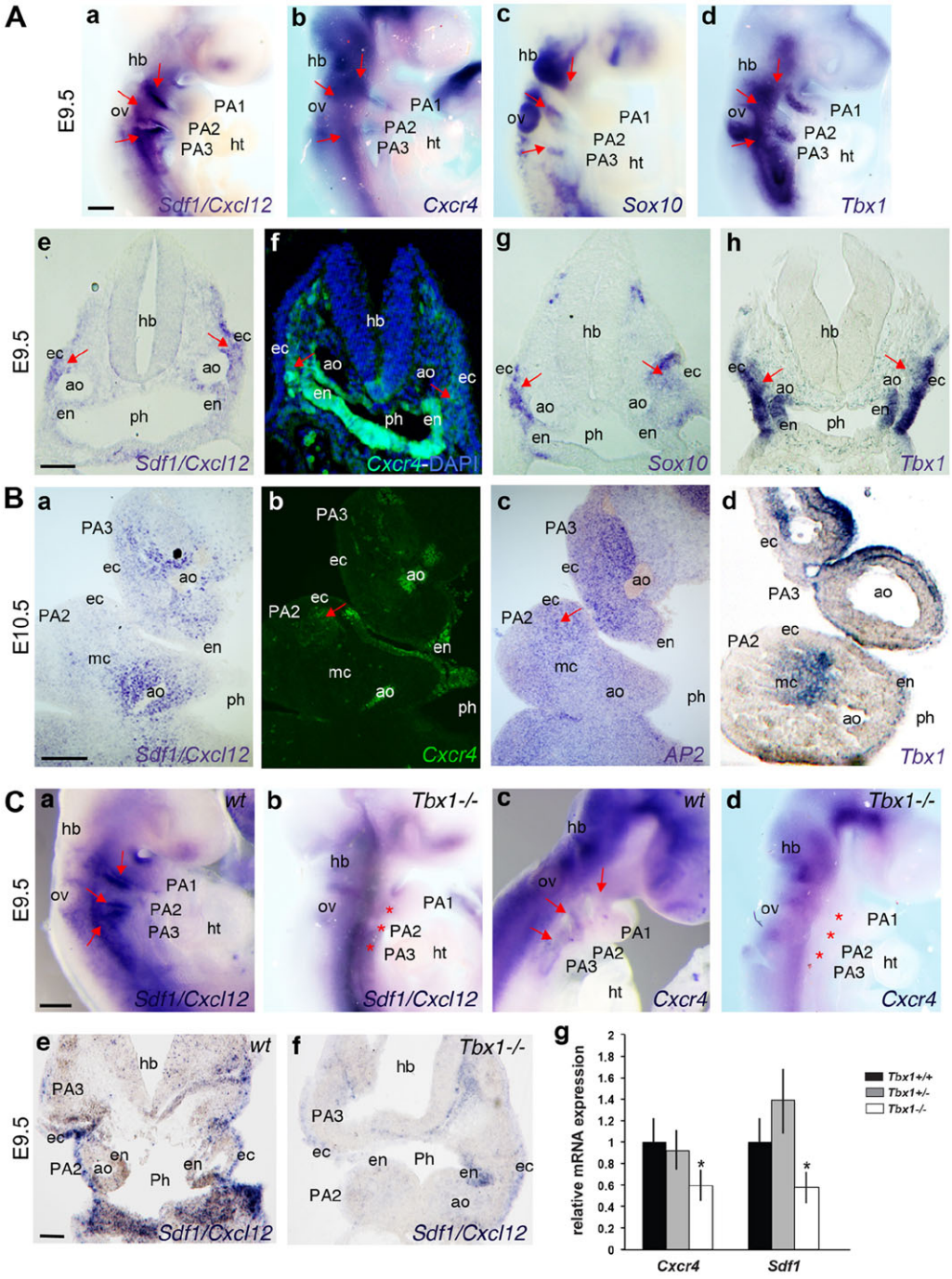

Fig. 1. *Cxcr4* and *Sdf1* are genetically downstream of *Tbx1* during PA colonization by pharyngeal NCs in mouse. (A,B) *Sdf1*, *Cxcr4*, *Sox10*, *AP2* (TFAP2A) and *Tbx1* expression at E9.5 and E10.5. Whole-mount views of labeled embryos (Aa-Ad), transverse sections through PA2 (Ae-Ah) and horizontal sections through PA2-3 (Ba-Bd) hybridized with probes for *Sdf1*, *Cxcr4*, *Sox10*, *AP2* and *Tbx1*. Af and Bb show GFP visualization in CXCR4-EGFP transgenic embryos allowing the detection of CXCR4-expressing cells. Arrows point to streams of pharyngeal NCs colonizing the PAs. Scale bars: 50 µm. (C) *Sdf1* and *Cxcr4* expression in *Tbx1* mutant mice. Whole-mount views (Ca-Cd) and transverse sections through PA2 (Ce,Cf) of wild-type (wt) and Tbx1$^{-/-}$ embryos hybridized with probes for *Sdf1* and *Cxcr4*. Arrows point to streams of pharyngeal NCs and asterisks indicate diminished expression of *Sdf1* and *Cxcr4* in PAs. Scale bars: 50 µm. (Cg) RT-qPCR analyses of *Cxcr4* and *Sdf1* in *Tbx1*$^{+/+}$, *Tbx1*$^{+/-}$ and *Tbx1*$^{-/-}$ E9.5 embryos. Error bars indicate s.d. **P*<0.05. ao, aortic arch; ec, ectoderm; en, endoderm; hb, hindbrain; ht, heart; mc, mesodermal core; ov, otic vesicle; PA1-3: pharyngeal arches 1-3; ph, pharynx.

Ah). At E10.5 (Fig. 1Ba-Bd), *Cxcr4* expression decreased gradually in NCs occupying the PA and became restricted to some blood vessels, including aortic arches (Fig. S1), whereas *Sdf1* and *Tbx1* expression shifted to the pharyngeal mesoderm, where they partially overlapped in the mesodermal core. This indicates that *Tbx1* and *Sdf1* expression patterns overlap transiently in the ectoderm and pharyngeal endoderm during pharyngeal NC migration. To address the question of the *Tbx1* regulation of SDF1 signaling, *Sdf1* and *Cxcr4* expressions were studied in *Tbx1* mouse mutants (Fig. 1C). Analysis of whole embryos (Fig. 1Ca-Cd) and cross-sections through the PA (Fig. 1Ce,Cf) at E9.5 showed a strong reduction of both *Sdf1* and *Cxcr4* expression in the PA of *Tbx1* mutants compared with wild-type embryos. This result was confirmed by the quantification of *Cxcr4* and *Sdf1* messages in *Tbx1* mouse mutants, which showed a decrease of nearly 50% in the transcriptional activity of both genes in the *Tbx1*$^{-/-}$ mouse, compared with their wild-type or heterozygote littermates (Fig. 1Cg). Thus, our data reveal that in mouse, both *Cxcr4* and *Sdf1* are downstream of *Tbx1* in the genetic cascade regulating PA development.

Sdf1 and *Cxcr4* expression patterns correlate with pharyngeal NC migration to PAs in chick

We turned to the chick model to determine whether CXCR4 signaling might be involved in pharyngeal NC development. Indeed,

Development (2016) 143, 582-588 doi:10.1242/dev.126573

NC migration and differentiation have been thoroughly examined in chick, as in mouse, and pharyngeal NCs can be precisely targeted using electroporation of the corresponding neural tube level, in contrast to mouse for which NC promoters available for conditional knockouts do not specifically target the pharyngeal NCs. We showed previously that cardiac NCs migrating towards PA3-4 express *Cxcr4* and that *Sdf1* exhibits a complementary pattern in the ectoderm along their migratory route (Escot et al., 2013). We therefore investigated the expression patterns of *Sdf1* and *Cxcr4* in relation to *Tbx1* in pharyngeal NCs populating PA1-2 (Fig. 2A; Le Douarin and Kalcheim, 1999). Immunohistology and *in situ* hybridization analyses revealed that NCs migrating into PA1-2 (Fig. 2B,C; Fig. S2) expressed *Cxcr4* in proximity to *Sdf1*-expressing ectodermal and pharyngeal endodermal cells, exactly as observed for those invading PA3-4. At this level, *Sdf1* and *Tbx1* expression patterns overlapped in both tissues. At E2.5, once NCs had colonized the PAs, they gradually downregulated *Cxcr4* expression, concommitant with *Sdf1* and *Tbx1* expression being shifted from the ectoderm to the pharyngeal mesoderm (Fig. 2D). From E3.5, *Cxcr4* became restricted to endothelia within the aortic arches (Fig. 2E; Fig. S1). Thus, in contrast to other NC populations, e.g. at truncal levels (Fig. S3) or along the digestive tract (Escot et al., 2013), and similarly to mouse, chick pharyngeal NCs share in common a conspicuous *Cxcr4* expression throughout their migration along paths lined by *Sdf1*- and *Tbx1*-expressing cells, making SDF1 signaling a potential candidate for the NC anomalies observed in DGS patients.

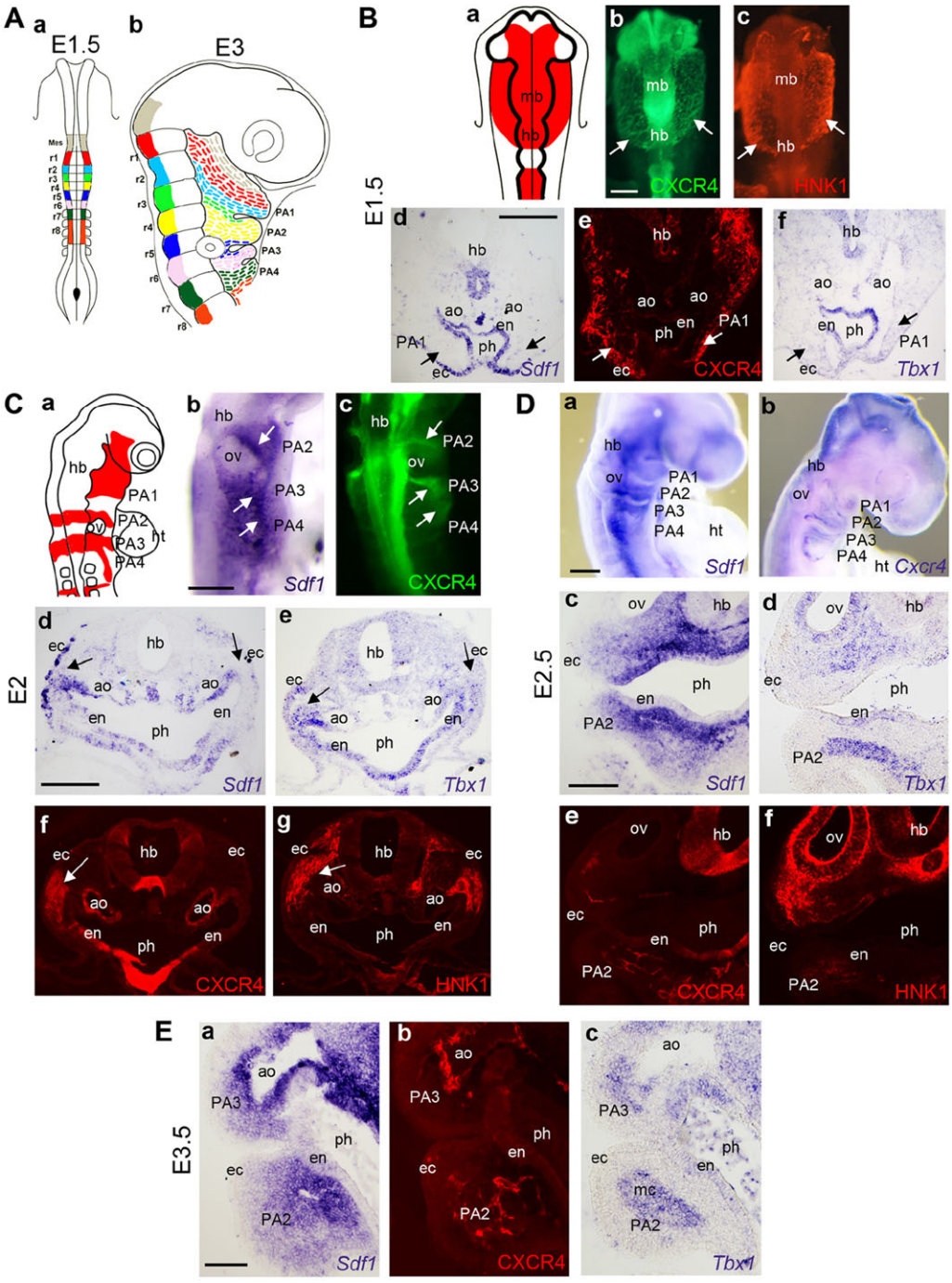

Fig. 2. *Sdf1* and *Cxcr4* expression profiles during pharyngeal NC migration in chick. (A) Fate map of pharyngeal NCs in chick. Color-coded schemas showing the posterior midbrain (Mes) and the hindbrain rhombomeres (r1 to r8) at E1.5 (Aa) and the location of corresponding NCs in PA1-4 at E3 (Ab). (B,C) *Sdf1*, CXCR4 and *Tbx1* expression during early pharyngeal NC migration towards PA1 at E1.5 (B) and PA2-4 at E2 (C). Schemas depict NC distribution (red) at these stages (Ba,Ca). Whole-mount views of labeled embryos (Bb,Bc; Cb,Cc) and cross-sections through PA1 (Bd-Bf) and PA2 (Cd-Cg) hybridized for *Sdf1* and *Tbx1* and immunolabeled for CXCR4 and the specific chick NC antibody HNK1 are shown. Arrows point at migrating NCs identified by HNK1. (D,E) *Sdf1*, *Cxcr4* and *Tbx1* expression during late PA colonization by NCs at E2.5-E3.5. Whole-mount views of embryos (Da, Db), cross-sections through PA2 (Dc-Df) and horizontal sections through PA2-3 (Ea-Ec) hybridized with probes for *Sdf1, Cxcr4* and *Tbx1* and immunolabeled for CXCR4 and HNK1. Scale bars: 100 µm. ao, aortic arch; ec, ectoderm; en, endoderm; hb, hindbrain; ht, heart; mb, midbrain; mc, mesodermal core; ov, otic vesicle; ph, pharynx, PA1-4: pharyngeal arches 1-4.

Development (2016) 143, 582-588 doi:10.1242/dev.126573

Disruption of CXCR4 signals in chick pharyngeal NCs causes craniofacial, glandular and neural defects

To determine whether defects in CXCR4 signaling might be responsible for the NC anomalies in DGS, CXCR4 activity was inhibited in pharyngeal NCs in chick and the consequences on the formation of their major derivatives analyzed (Fig. 3A). We previously reported that disrupting this signaling pathway in cardiac NCs results in cardiac defects similar to those found in DGS (Escot et al., 2013). We therefore investigated the other tissues known to be affected in this pathology. Using *in ovo* electroporation,

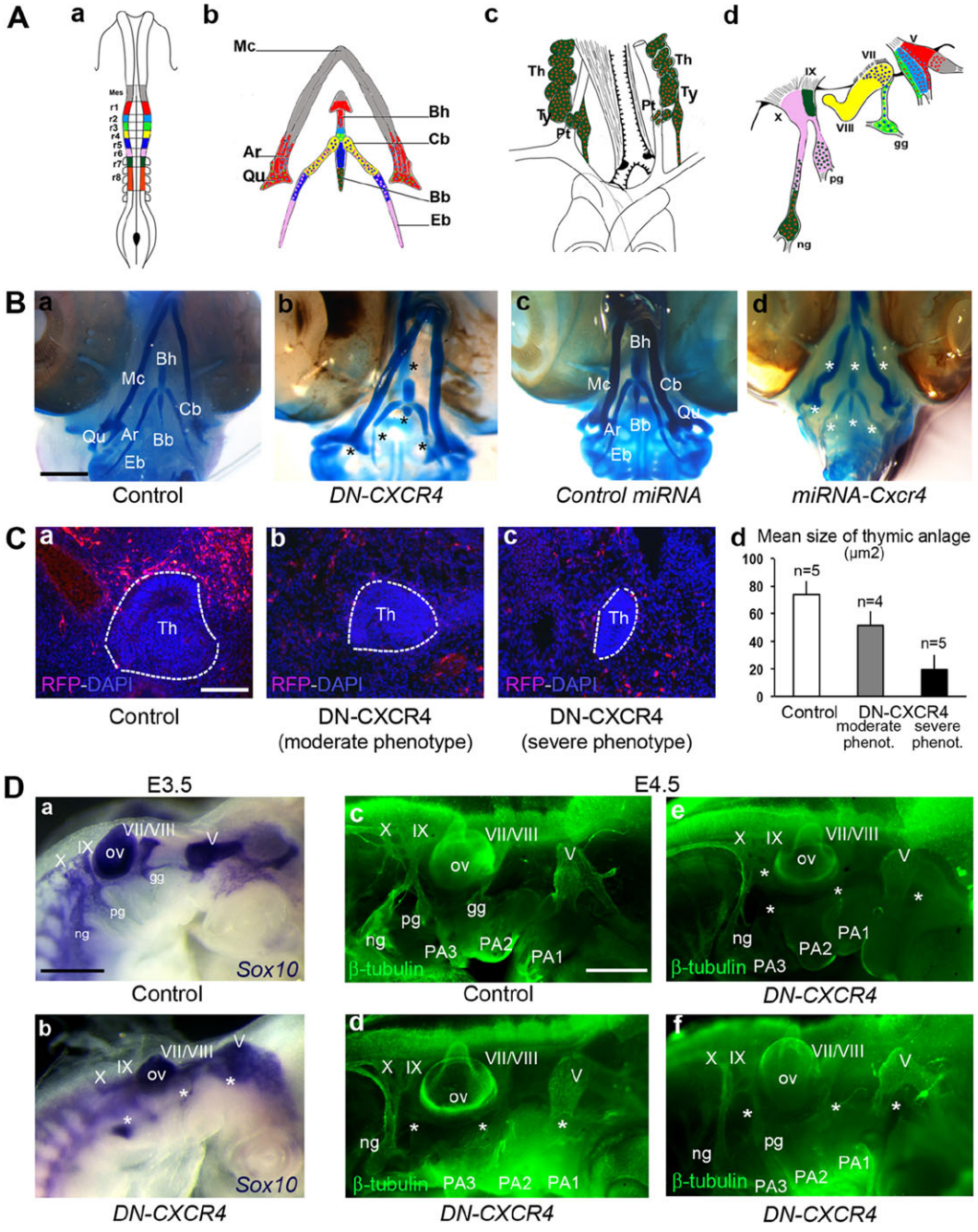

Fig. 3. Defective CXCR4 signaling in pharyngeal NCs leads to abnormal craniofacial derivatives. (A) Fate map of neural, skeletal and glandular derivatives of pharyngeal NCs. Color-coded schemas showing the posterior midbrain (Mes) and the hindbrain rhombomeres (r1 to r8) at E1.5 (Aa) and the contribution of the corresponding NCs to the skeleton of the lower jaw and the hyoid bones at E9.5 (Ab), to the connective components of the thymus, thyroid and parathyroid at E12 (Ac), and to the cranial ganglia and nerves at E4.5 (Ad). (B) Skeletal defects. Alcian Blue and Alizarin Red staining of head skeleton showing anomalies of the lower jaw and hyoid bone (asterisks) obtained at E9.5 in *DN-CXCR4* and *miRNA-Cxcr4* embryos. (C) Impaired development of the thymic primordium. RFP visualization and DAPI staining on cross-sections through thymic primordia at E7.5 (Ca-Cc) and quantification of their mean size (Cd), illustrating their atrophy in the absence of surrounding NCs in *DN-CXCR4* embryos. Scale bar: 50 µm. Error bars represent s.d. (D) Cranial ganglia and nerve anomalies. Lateral views of control and *DN-CXCR4* embryos revealing *Sox10* expression at E3.5 (Da,Db) and β-tubulin expression at E4.5 (Dc-Df), showing mispatterning of cranial ganglia and nerves (asterisks) in *DN-CXCR4* specimens. Scale bars: 300 µm. Ar, articular bone; Bb, basibranchial; Bh, basihyal; Cb, ceratobranchial; Eb, epibranchial; gg, geniculate ganglion; Mc, Meckel's cartilage; ng, nodose ganglion; ov, otic vesicle; PA1-3: pharyngeal arches; pg, petrosal ganglion; Pt, parathyroid; Qu, quadrate; Th, thymus; Ty, thyroid; V, VII, VIII, IX and X: trigeminal, facial, vestibuloacoustic, glossopharyngeal and vagal nerves, respectively.

Development (2016) 143, 582-588 doi:10.1242/dev.126573

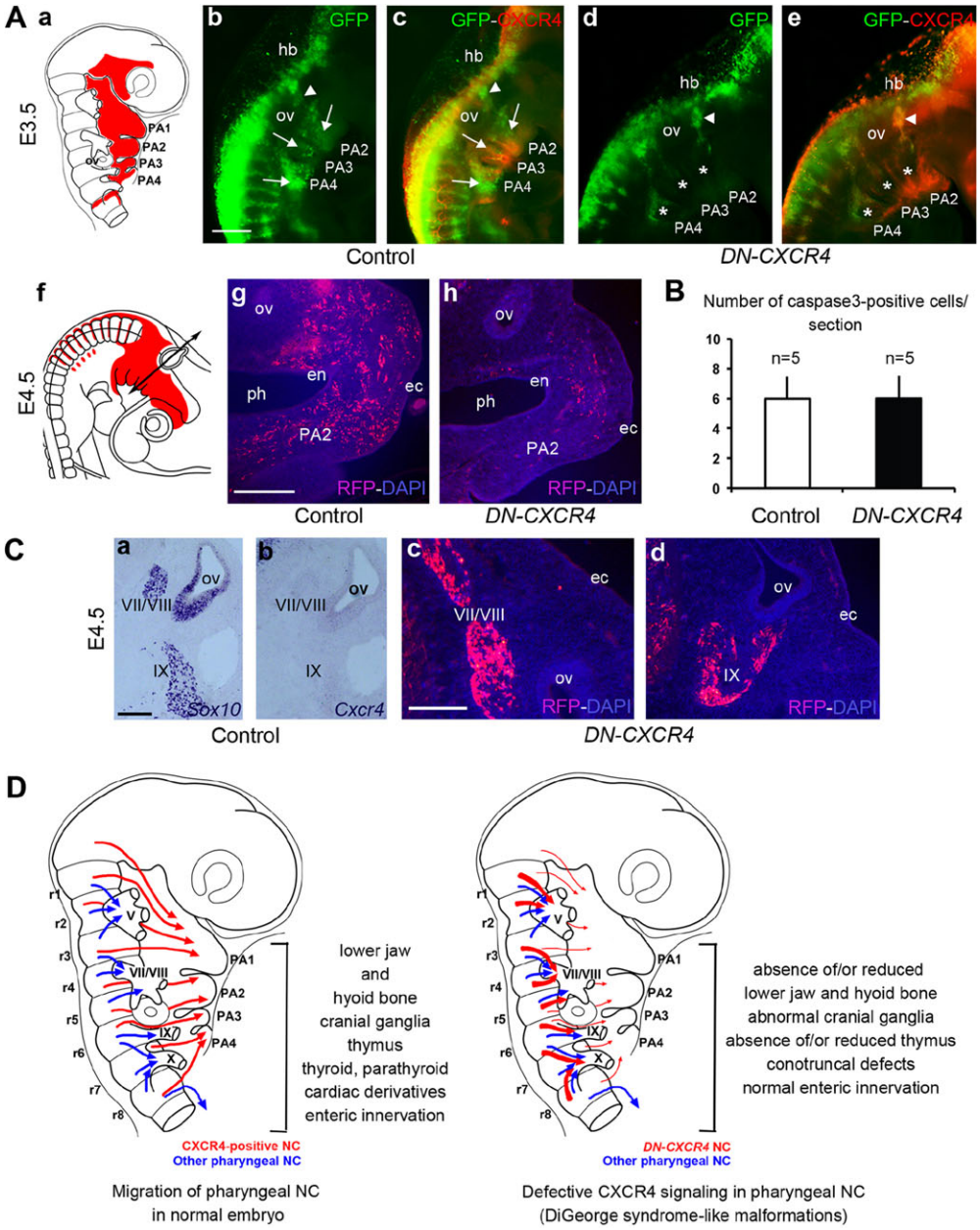

Fig. 4. Craniofacial and neural anomalies after disruption of CXCR4 signaling result from early misrouting of pharyngeal NCs. (A,B) Pharyngeal NC migration defects in *DN-CXCR4* embryos. (Aa,Af) Schematic representations of NC distribution in PAs (in red) at E3.5 and E4.5. (Ab-Ae) GFP visualization and CXCR4 immunodetection in whole-mount control and *DN-CXCR4* embryos at E3.5. Arrows point to pharyngeal NC streams invading PA2-4 in the control and asterisks mark their reduction in *DN-CXCR4* embryos. Arrowheads point to the presence of *CXCR4*-expressing NCs in the vestibuloacoustic ganglion in *DN-CXCR4* embryos and their absence in controls. Scale bar: 200 µm. (Ag,Ah) RFP visualization and DAPI staining in cross-sections through PA2 in control and *DN-CXCR4* embryos at E4.5, showing NC diminution in PA2. Scale bar: 100 µm. (B) Quantification of activated caspase3-positive NCs in the PAs of control and *DN-CXCR4* embryos at E3.5. Error bars represent s.d. (C) NC misrouting to cranial ganglia in E4.5 *DN-CXCR4* embryos. (Ca,Cb) *In situ* hybridizations for *Sox10* and *Cxcr4* on horizontal sections through cranial ganglia at E3 showing that normally, cranial ganglia and nerves do not contain *Cxcr4*-expressing NCs. (Cc,Cd) RFP visualization and DAPI staining on transverse sections anterior (Cc) and posterior (Cd) to the otic vesicle showing numerous RFP-positive cells (i.e. *DN-CXCR4*-transfected cells) misrouted into cranial ganglia of *DN-CXCR4* embryos. Scale bars: 100 µm. (D) Model of pharyngeal NC migration defects as a result of CXCR4 signaling misregulation, thought to be at the origin of most of the cardiocraniofacial anomalies observed in DGS. Thickness of arrows indicates the relative number of NCs migrating into PAs or cranial ganglia. ec, ectoderm; en, endoderm; hb, hindbrain; ov, otic vesicle; PA1-4, pharyngeal arches 1-4; ph, pharynx; r1-r8, rhombomeres 1-8; V, VII, VIII, IX and X: trigeminal, facial, vestibuloacoustic, glossopharyngeal and vagal ganglia, respectively.

we expressed in pharyngeal NCs either a miRNA against *Cxcr4* (*miRNA-Cxcr4*, Fig. S5) or a dominant-negative form of *Cxcr4* (*DN-CXCR4*) lacking the C-terminus sequences necessary for chemotactic migration (Ahr et al., 2005; Cronshaw et al., 2010). First, we searched for craniofacial dysmorphogenesis due to palate and jaw anomalies, a prominent trait of DGS patients (Fukui et al., 2000; Karpinski et al., 2014). Heads of chick embryos were collected at E9.5 and the jaw anatomy examined. All controls exhibited normal heads (n=18), whereas most embryos in which CXCR4 signaling was affected exhibited anomalies of the lower jaw and hyoid bone, with frequently shortened or absent basibranchial, epibranchial and ceratobranchial bones and Meckel's cartilage, all

Development (2016) 143, 582-588 doi:10.1242/dev.126573

derived from NCs that populate PA2-3 (Fig. 3A,B; Table S1; *n*=16). As described previously for the cardiac defects (Escot et al., 2013), jaw anomalies were more frequent in *DN-CXCR4*-electroporated embryos than in *miRNA-Cxcr4* ones (Table S1), owing to the earlier effect of *DN-CXCR4* on NC migration (Escot et al., 2013). For this reason, we focused our following phenotypic analyses on *DN-CXCR4*-electroporated embryos.

One of the NC-related anomalies found in DGS patients is thymus hypoplasia, which is also the origin of immune disorders (Shprintzen, 2008). Indeed, NCs migrating to PA4 contribute to connective tissues and pericytes of the thymus (Fig. 3A), and are essential for the development of the thymic epithelium (Kuratani and Bockman, 1990). Analysis of embryos at E7.5, when the thymus anlage becomes recognizable, revealed smaller thymus primordia in *DN-CXCR4*-electroporated animals than in controls. The mean surface area of the thymus on transverse sections was reduced from 30% in the milder phenotypes up to 60% in the most severe cases (Fig. 3C; *n*=9).

Finally, disrupted cranial nerves have been reported in the *LgDel* mouse, possibly accounting for the dysphagia observed in children diagnosed with DGS (Karpinski et al., 2014). Pharyngeal NCs contribute to some of the major cranial sensory ganglia, i.e. V (trigeminal), VII-VIII (facial and vestibuloacoustic) and IX-X (glossopharyngeal and vagal) (Ayer-Le Lievre and Le Douarin, 1982) (Fig. 3A). *In situ* hybridization for *Sox10* in whole embryos showed considerable mispatterning of cranial sensory ganglia in *DN-CXCR4*-embryos at E3.5, with some of them partially fused and others atrophied or missing (Fig. 3Da,Db; *n*=11). These abnormalities resulted at later stages in a variety of phenotypes, characterized by missing, fused or misrouted cranial nerves (Fig. 3Dc-Df; *n*=8).

Taken together, our results demonstrate that disrupting CXCR4 signals in pharyngeal NCs induces a large spectrum of abnormalities in their skeletal, neuronal and glandular derivatives, which, in addition to the cardiac defects already reported (Escot et al., 2013), recapitulate the defects described in mouse models and DGS patients (Funato et al., 2015; Karpinski et al., 2014; Vitelli et al., 2002).

Craniofacial and neural anomalies after disruption of CXCR4 signaling result from pharyngeal NC misrouting

We then investigated how and when anomalies found in pharyngeal NC derivatives upon disruption of CXCR4 signals were generated. Analysis of NC distribution at E3.5 revealed that in *DN-CXCR4*-electroporated embryos, NCs initiated migration from the neural tube, but very few reached PA2-4, whereas control embryos showed massive NC colonization (Fig. 4Aa-Ae). At E4.5, in *DN-CXCR4*-electroporated embryos, PAs remained almost devoid of NCs (Fig. 4Af-Ah; *n*=8), although apoptosis was not increased during migration (Fig. 4B; *n*=5), thereby revealing that the colonization defect did not result from cell death or delayed migration. Interestingly, at both at E3.5 (*n*=6) and E4.5 (*n*=8) numerous *DN-CXCR4*-positive NCs were detected in cranial ganglia VII/VIII and IX, which are normally not colonized by CXCR4-expressing NCs (Fig. 4C). This indicates that NC depletion in PAs of *DN-CXCR4*-expressing embryos resulted from misrouted NC migration, consecutive to the inhibition of CXCR4 chemotactic activity. To validate this interpretation, we analyzed the migratory response of pharyngeal NCs to an ectopic source of *Sdf1*. When misexpressed in the neural tube, *Sdf1* caused misrouting of pharyngeal NCs, resulting in their massive accumulation along the neural tube and their depletion from PAs (Fig. S4). These results also provide an explanation for why cranial sensory ganglia are affected in *DN-CXCR4*-embryos although they do not rely on SDF1/CXCR4 signaling for their formation.

Conclusion

In conclusion, our study suggests a model in which *Tbx1* expressed in the lateral ectoderm and pharyngeal endoderm at early stages of pharyngeal NC migration might regulate *Sdf1* expression and consequently the CXCR4-mediated response to SDF1 signals in pharyngeal NCs, thereby controlling their chemotactic guidance towards the PAs. Inhibition of CXCR4 activity results in major defects in the cardiocraniofacial derivatives of pharyngeal NCs that phenocopy most anomalies of the *Tbx1* mouse mutant and congenital malformations observed in DGS (Fig. 4D). Taken together with the recent results showing functional defects of CXCR4 signaling in the brain of the *LgDel* and *Df1* mouse models (Meechan et al., 2012; Toritsuka et al., 2013), our study underlines the possibility of a pivotal role for the SDF1/CXCR4 axis in DGS etiology.

MATERIALS AND METHODS

Embryos

Fertilized chick eggs were from commercial sources and green fluorescent protein positive (GFP^+) transgenic chicken eggs (McGrew et al., 2008) from the Roslin Institute (University of Edinburgh, UK). Embryos were staged according to embryonic day of development. The transgenic mouse line [strain Tg(Cxcr4-ECFP)CD73Gsat/Mmucd, developed by the GENSAT project; NINDS contract N01Nso2331 to Rockefeller University, NY, USA] was purchased from Mutant Mouse Resource Research Centers. Mice carrying the $Tbx1^{+/-}$ allele were used and genotyped as described previously (Jerome and Papaioannou, 2001). All mutants were maintained in a predominantly C57BL/6 genetic background. Mouse care and procedures were in accordance with national and European laws.

Chick embryo manipulations

Grafting and *in ovo* electroporation experiments were performed as described (Escot et al., 2013). For grafting, hindbrains from GFP^+ transgenic chick donors at the 5-somite stage (30 h of development) were excised after enzymatic treatment and transplanted isotopically and isochronically into chick hosts *in ovo*, in which their equivalents have been removed surgically. For electroporations, expression plasmids described previously (Escot et al., 2013; supplementary materials and methods) were mixed with plasmids encoding GFP or RFP and microinjected into the neural tube lumen of 5-somite-stage embryos at the midbrain and hindbrain levels. Electrodes (CUY610 platinum-coated, Sonidel, Ireland) were applied onto the vitelline membrane on either side of the appropriate neural tube region and five square pulses (20 V, 50 ms length, 500 ms gap) were delivered. For the analysis of pharyngeal NC derivatives, pulses were delivered bilaterally to electroporate both sides of the neural tube. Embryos were re-incubated for up to 8 days after electroporation, harvested in PBS and monitored for GFP or RFP fluorescence at the appropriate axial levels. The efficiency of the transfections was verified on whole-mount samples or sections by *in situ* hybridization for *Sdf1* and immunofluorescence labeling for CXCR4.

Immunostaining, *in situ* hybridization and histological analyses

In situ hybridizations and immunostainings on whole embryos or sections were performed as described (Escot et al., 2013), using the following riboprobes: *Sox10* (P. Scotting, Queen's Medical Center, Nottingham), *Sdf-1* and *Cxcr4* (both produced from EST clones) (Escot et al., 2013), mouse *Tbx1* (V. Papaioannou, Columbia University Medical Center, New York), chick *Tbx1* (produced by PCR from the mouse Tbox domain conserved in chick) (Garg et al., 2001) and antibodies: anti-cleaved caspase-3 (1:100; 9664, Cell Signaling), anti-NC1/HNK1 (1:10; Tucker et al., 1984), anti-TuJ1 (1:300; 1637, Chemicon), anti-GFP (1:500; 1814460, Roche) and anti-chicken CXCR4 (1:1000; Escot et al., 2013). Nuclei were visualized

Development (2016) 143, 582-588 doi:10.1242/dev.126573

with DAPI (Sigma). For craniofacial skeleton analyses, heads were fixed in acetic acid and skeletons visualized using Alcian Blue and Alizarin Red.

Real-time RT-qPCR

The pharyngeal region of E9.5 embryos were dissected out from wild-type, *Tbx1*$^{+/-}$ and *Tbx1*$^{-/-}$ mutant mice. RT-qPCR was performed as described (Odelin et al., 2014) using the following primers: 5′-CCCCACAACTCTTCCATTCT-3′, 5′-GCAGGAGTGATAGGGGTCAT-3′ for *Tbx1*; 5′-TTGCCGACTATGCCAGTCAA-3′, 5′-CCGGGATGAAAACGTCCAT-3′ for *Cxcr4*; and 5′-CACTCCAAACTGTGCCCTTCA-3′, 5′-CACTTTAGCTTCGGGTCAATGC-3′ for *Sdf1*. RT-qPCR was performed using LightCycler 480 SYBR Green I Master mix (Roche) and cDNA synthesized using first-strand cDNA synthesis kit (Roche) from embryonic RNAs isolated using the NucleoSpin RNA/Protein Kit (Macherey-Nagel). Expression levels between wild-type (n=8), *Tbx1*$^{+/-}$ (n=6) and *Tbx1*$^{-/-}$ (n=6) embryos were calculated by the comparative cycle threshold (ΔΔCT) method. Each experiment was performed in triplicate for each genotype and normalized to endogenous *Tbp* housekeeping gene. Normalized expression levels in the control (*Tbx1*$^{+/+}$) were set to 1.0 for each gene. Student's t-test was used to determine statistical significance.

Quantitative analyses

Apoptosis quantitation was performed as described (Escot et al., 2013). The size of thymic primordia was determined using the Nikon NIS Elements imaging software. The outline of the primordium was delineated on each section to calculate its area. The total primordium area in each embryo was calculated by summing the areas of the primordium on each section. Statistical significances were evaluated using Student's t-test.

Acknowledgements

We thank S. Gournet for illustrations; our colleagues for probes and antibodies; and the GFP^{+} transgenic egg resource at the Roslin Institute.

Competing interests

The authors declare no competing or financial interests.

Author contributions

S.E. performed experiments and analyzed data. C.B. performed experiments. E.F. and S.Z. performed the analyses on mouse embryos. C.F.-T. and J.-L.D. designed experiments and wrote the manuscript.

Funding

This work was supported by the French National Centre for Scientific Research (CNRS); the Université Pierre et Marie Curie; and the Association Française contre les myopathies [grant no. 11,405]. S.E. was a recipient of a doctoral fellowship from the Ministère de l'Enseignement Supérieur et de la Recherche.

Supplementary information

Supplementary information available online at
http://dev.biologists.org/lookup/suppl/doi:10.1242/dev.126573/-/DC1

References

Ahr, B., Denizot, M., Robert-Hebmann, V., Brelot, A. and Biard-Piechaczyk, M. (2005). Identification of the cytoplasmic domains of CXCR4 involved in Jak2 and STAT3 phosphorylation. *J. Biol. Chem.* **280**, 6692-6700.

Ayer-Le Lievre, C. S. and Le Douarin, N. M. (1982). The early development of cranial sensory ganglia and the potentialities of their component cells studied in quail-chick chimeras. *Dev. Biol.* **94**, 291-310.

Calmont, A., Ivins, S., Van Bueren, K. L., Papangeli, I., Kyriakopoulou, V., Andrews, W. D., Martin, J. F., Moon, A. M., Illingworth, E. A., Basson, M. A. et al. (2009). Tbx1 controls cardiac neural crest cell migration during arch artery development by regulating Gbx2 expression in the pharyngeal ectoderm. *Development* **136**, 3173-3183.

Castellanos, R., Xie, Q., Zheng, D., Cvekl, A. and Morrow, B. E. (2014). Mammalian TBX1 preferentially binds and regulates downstream targets via a tandem T-site repeat. *PLoS ONE* **9**, e95151.

Cronshaw, D. G., Nie, Y., Waite, J. and Zou, Y.-R. (2010). An essential role of the cytoplasmic tail of CXCR4 in G-protein signaling and organogenesis. *PLoS ONE* **5**, e15397.

Escot, S., Blavet, C., Härtle, S., Duband, J.-L. and Fournier-Thibault, C. (2013). Misregulation of SDF1-CXCR4 signaling impairs early cardiac neural crest cell migration leading to conotruncal defects. *Circ. Res.* **113**, 505-516.

Fukui, N., Amano, A., Akiyama, S., Daikoku, H., Wakisaka, S. and Morisaki, I. (2000). Oral findings in DiGeorge syndrome: clinical features and histologic study of primary teeth. *Oral Surg. Oral Med. Oral Pathol. Oral Radiol. Endod.* **89**, 208-215.

Funato, N., Nakamura, M., Richardson, J. A., Srivastava, D. and Yanagisawa, H. (2015). Loss of Tbx1 induces bone phenotypes similar to cleidocranial dysplasia. *Hum. Mol. Genet.* **24**, 424-435.

Garg, V., Yamagishi, C., Hu, T., Kathiriya, I. S., Yamagishi, H. and Srivastava, D. (2001). Tbx1, a DiGeorge syndrome candidate gene, is regulated by sonic hedgehog during pharyngeal arch development. *Dev. Biol.* **235**, 62-73.

Jerome, L. A. and Papaioannou, V. E. (2001). DiGeorge syndrome phenotype in mice mutant for the T-box gene, Tbx1. *Nat. Genet.* **27**, 286-291.

Karpinski, B. A., Maynard, T. M., Fralish, M. S., Nuwayhid, S., Zohn, I. E., Moody, S. A. and LaMantia, A.-S. (2014). Dysphagia and disrupted cranial nerve development in a mouse model of DiGeorge (22q11) deletion syndrome. *Dis. Model. Mech.* **7**, 245-257.

Kirby, M. L., Gale, T. F. and Stewart, D. E. (1983). Neural crest cells contribute to normal aorticopulmonary septation. *Science* **220**, 1059-1061.

Kochilas, L., Merscher-Gomez, S., Lu, M. M., Potluri, V., Liao, J., Kucherlapati, R., Morrow, B. and Epstein, J. A. (2002). The role of neural crest during cardiac development in a mouse model of DiGeorge syndrome. *Dev. Biol.* **251**, 157-166.

Kuratani, S. and Bockman, D. E. (2000). Impaired development of the thymic primordium after neural crest ablation. *Anat. Rec.* **190**, 185-190.

Le Douarin, N. and Kalcheim, C. (1999). The neural crest: a source of mesenchymal cells. In *The Neural Crest* (ed. B. L. Bard, P. W. Barlow and D. L. Kirk), pp. 60-152. Cambridge University Press.

Lindsay, E. A., Vitelli, F., Su, H., Morishima, M., Huynh, T., Pramparo, T., Jurecic, V., Ogunrinu, G., Sutherland, H. F., Scambler, P. J. et al. (2001). Tbx1 haploinsufficieny in the DiGeorge syndrome region causes aortic arch defects in mice. *Nature* **410**, 97-101.

Ma, Q., Jones, D., Borghesani, P. R., Segal, R. A., Nagasawa, T., Kishimoto, T., Bronson, R. T. and Springer, T. A. (1998). Impaired B-lymphopoiesis, myelopoiesis, and derailed cerebellar neuron migration in CXCR4- and SDF-1-deficient mice. *Proc. Natl. Acad. Sci. USA* **95**, 9448-9453.

McGrew, M. J., Sherman, A., Lillico, S. G., Ellard, F. M., Radcliffe, P. A., Gilhooley, H. J., Mitrophanous, K. A., Cambray, N., Wilson, V. and Sang, H. (2008). Localised axial progenitor cell populations in the avian tail bud are not committed to a posterior Hox identity. *Development* **135**, 2289-2299.

Meechan, D. W., Tucker, E. S., Maynard, T. M. and LaMantia, A.-S. (2012). Cxcr4 regulation of interneuron migration is disrupted in 22q11.2 deletion syndrome. *Proc. Natl. Acad. Sci. USA* **109**, 18601-18606.

Mesbah, K., Rana, M. S., Francou, A., van Duijvenboden, K., Papaioannou, V. E., Moorman, A. F., Kelly, R. G. and Christoffels, V. M. (2012). Identification of a Tbx1/Tbx2/Tbx3 genetic pathway governing pharyngeal and arterial pole morphogenesis. *Hum. Mol. Genet.* **21**, 1217-1229.

Odelin, G., Faure, E., Kober, F., Maurel-Zaffran, C., Théron, A., Coulpier, F., Guillet, B., Bernard, M., Avierinos, J.-F., Charnay, P. et al. (2014). Loss of Krox20 results in aortic valve regurgitation and impaired transcriptional activation of fibrillar collagen genes. *Cardiovasc. Res.* **104**, 443-455.

Puech, A., Saint-Jore, B., Funke, B., Gilbert, D. J., Sirotkin, H., Copeland, N. G., Jenkins, N. A., Kucherlapati, R., Morrow, B. and Skoultchi, A. I. (1997). Comparative mapping of the human 22q11 chromosomal region and the orthologous region in mice reveals complex changes in gene organization. *Proc. Natl. Acad. Sci. USA* **94**, 14608-14613.

Scambler, P. J. (2010). 22q11 deletion syndrome: a role for TBX1 in pharyngeal and cardiovascular development. *Pediatr. Cardiol.* **31**, 378-390.

Shprintzen, R. J. (2008). Velo-cardio-facial syndrome: 30 Years of study. *Dev. Disabil. Res. Rev.* **14**, 3-10.

Toritsuka, M., Kimoto, S., Muraki, K., Landek-Salgado, M. A., Yoshida, A., Yamamoto, N., Horiuchi, Y., Hiyama, H., Tajinda, K., Keni, N. et al. (2013). Deficits in microRNA-mediated Cxcr4/Cxcl12 signaling in neurodevelopmental deficits in a 22q11 deletion syndrome mouse model. *Proc. Natl. Acad. Sci. USA* **110**, 17552-17557.

Tran, P. B., Banisadr, G., Ren, D., Chenn, A. and Miller, R. J. (2007). Chemokine receptor expression by neural progenitor cells in neurogenic regions of mouse brain. *J. Comp. Neurol.* **1033**, 1007-1033.

Tucker, G. C., Aoyama, H., Lipinski, M., Tursz, T. and Thiery, J. P. (1984). Identical reactivity of monoclonal antibodies HNK-1 and NC-1: conservation in vertebrates on cells derived from the neural primordium and on some leukocytes. *Cell Differ.* **14**, 223-230.

Vitelli, F., Morishima, M., Taddei, I., Lindsay, E. A. and Baldini, A. (2002). Tbx1 mutation causes multiple cardiovascular defects and disrupts neural crest and cranial nerve migratory pathways. *Hum. Mol. Genet.* **11**, 915-922.

Zhang, Z., Cerrato, F., Xu, H., Vitelli, F., Morishima, M. Vincentz, J., Furuta, Y., Ma, L., Martin, J. F., Baldini, A. et al. (2005). Tbx1 expression in pharyngeal epithelia is necessary for pharyngeal arch artery development. *Development* **132**, 5307-5315.